Supplementary Information (SI) for Chemical Science.

Supplementary Information

Highly Efficient and Selective Sr^{2+} Capture Using Robust Two-Dimensional MOF Nanosheets Decorated with Cage-Like Cavities

Xiao-Ran Jia,[†] Zi-Xuan Gao,[†] Hai-Ming Fei,[§] Li-Juan Lan,[†] Cai-Xia Yu,[*,†] Yong Qian[*,‡] and Lei-Lei Liu[*,†]

[†] *School of Environmental and Material Engineering, Yantai University, Yantai 264005, P. R. China*

[‡] *State Key Laboratory of Nuclear Resources and Environment, East China University of Technology, Nanchang, Jiangxi 330013, P. R. China*

[§] *College of Chemical Engineering, Huaqiao University, Xiamen 361021, P. R. China*

* Corresponding authors: yucaixiachem@163.com; yqianecit@163.com; liuleileimail@163.com

Table of Contents

Materials and physical measurements

General procedure

The ligand 5,11,17,23-tetra-tert-butyl-25,26,27,28-tetrakis[(carboxyl)methoxy]calix[4]arene (H_4L) was prepared according to the literature method.[1] All other chemicals and reagents were obtained from commercial sources and used as received. Powder X-ray diffraction (PXRD) was performed using a PANalytical X'Pert PRO MPD system (PW3040/60). Thermal analysis was performed with a Netzsch STA-449F3 thermogravimetric analyzer at a heating rate of 10 °C min^{-1} and a flow rate of 20 $\mathrm{cm}^3\ \mathrm{min}^{-1}$ (N_2). Fourier transform infrared (FT-IR) spectra were recorded on an IR Prestige 21. The FT-IR samples were prepared by blending the compound with KBr and compressing the mixture to obtain transparent sheets. Scanning electron microscopy (SEM) image was observed by the JSM-7610F (JEOL, Japan) apparatus working at an acceleration voltage of 10 kV. X-ray photoelectron spectroscopy (XPS) was measured on a Thermo Escalab 250 X-ray photoelectron spectrometer equipped with Al radiation as the probe (Kα, radiation).

Synthesis of $\{[Cu(H_2L)(H_2O)]\cdot 0.5H_2O\}_n$ (Cu-MOF-COOH)

$CuCl_2\cdot 2H_2O$ (5.4 mg, 0.032 mmol), H_4L (7.0 mg, 0.008mmol), and 6 mL MeCN/H_2O (2/1, V/V) were placed in 10 mL vial. After it was sealed, the vial was heated at 363 K for 48 hours, then slowly cooled to room temperature. The crystals of **Cu-MOF-COOH** were filtered and washed with MeCN thoroughly and then dried at room temperature.

Preparation of 2D Cu-MOF-COOH nanosheets

Firstly, the 3D bulk **Cu-MOF-COOH** was ground in an agate mortar for about 1 hour. Secondly, the ground 3D bulk **Cu-MOF-COOH** was activated by heating at 373 K (12 hours) under vacuum to remove the encapsulated solvent guests, which would destroy the interlayer interactions between the layers and facilitate further exfoliation. Thirdly, 50 mg of the as-prepared 3D bulk **Cu-MOF-COOH** was dispersed in 100 mL of MeOH/isopropanol (4/1, V/V) and sonicated in an ice-water bath for 6 hours. After sedimentation for 8 hours, the upper colloidal suspension was centrifugated at 10000 rpm at 278 K to get the exfoliated **Cu-MOF-COOH** nanosheets, which were collected and dried in the air.

X-ray crystal structure determination

Single X-ray diffraction intensities of crystal were collected on a CCD diffractometer at 100 K. All diffractometers were equipped with a graphite monochromated Mo-Kα radiation (λ = 0.71073). The structure was solved by the direct method and expanded with the Fourier technique. All calculations were performed with the SHELXL-97 package. The crystal data for **Cu-MOF-COOH** was summarized as follows: $C_{104}H_{128}Cu_2O_{27}$, Mr =1937.14, monoclinic, space group $P2_1/c$, a = 22.468(5) Å, b = 10.540(2) Å, c = 20.861(4) Å, α = 90°, β = 91.80(3)°, γ = 90°, V = 4937.6(17) Å^3, Z = 2, D_c = 1.304 g cm^{-3}, $F(000)$ = 2052.0 and μ = 0.507 mm^{-1}, 32898 reflections collected, 8684 unique (R_{int} = 0.0323). R_1 = 0.0354, wR_2 = 0.1014 and S = 1.043. Crystallographic data have been submitted to the Cambridge Structural Database with deposition number CCDC 2427696.

TEM and AFM characterizations

Before the characterizations of transmission electron microscopy (TEM) and atomic force microscopy (AFM), 3 mg of the as-prepared MOF was dispersed in 10 mL of MeOH/isopropanol (4/1, V/V) and sonicated in an ice-water bath for 6 hours. After sedimentation for 12 hours, the upper colloidal suspension of **Cu-MOF-COOH** nanosheets was dropped onto the holey carbon-coated carbon support copper grids and mica, respectively, and then naturally dried in air. The morphology of nanosheets was observed by field emission transmission electron microscopy (TEM, JEOL JEM 2100, Japan) at an acceleration voltage of 200 kV. The surface morphology and the height of nanosheets were obtained on a dimension edge microscope (AFM, Bruker Edge, Germany) equipped with a tapping mode.

Extraction experiments

Organic phase selection study

Although tert-butyl groups in **Cu-MOF-COOH** offer significant advantages in exfoliation (e.g., facilitating nanosheet formation), their inherent hydrophobicity confers chemical robustness to the nanosheets in aqueous environments but simultaneously impedes dispersibility in the aqueous phase. To circumvent this limitation, **Cu-MOF-COOH** nanosheets functionalized with tert-butyl groups were dispersed in organic solvents to enable efficient extraction of Sr^{2+} from aqueous solutions via an extraction strategy. This approach exploits the nanosheets' hydrophobicity to drive partitioning into the organic phase while permitting selective Sr^{2+} complexation or adsorption at the aqueous-organic interface, thereby enhancing extraction efficiency. The type and nature of the extraction solvent are pivotal in the extraction process, which influences not only the dispersion of the extractant but also its extraction behavior. To this end, we evaluated the impact of various organic phases on the efficacy of **Cu-MOF-COOH** nanosheets in extracting Sr^{2+}. As it is dangerous to use the ^{90}Sr compound in an unqualified laboratory, non-radioactive surrogate Sr^{2+} was used for the extraction experiments. Preliminary screening tests revealed that the extractants dispersed effectively in toluene, n-hexane, cyclohexane, chloroform ($CHCl_3$), and petroleum ether. To identify the optimal solvents for Sr^{2+} extraction, 7 mg of MOF nanosheets were dispersed in 10 mL of different organic phases with a certain content of Sr^{2+} solution (10 ppm; 15 mL). The extraction experiments were conducted at pH 10. After extraction, the phases were separated by standing for 12 hours. The aqueous phase samples were analyzed then filtered through a 0.22 μm membrane and measured using atomic absorption spectrometry (AAS) or inductively coupled plasma mass spectrometry (ICP-MS, Agilent 7800, USA). Results depicted in Figure S22 indicated that the solvents exhibit the following rank order in terms of extraction efficiency: toluene (99.34%) > $CHCl_3$ (87.83%) > n-hexane (78.02%) > cyclohexane (72.29%) > petroleum ether (62.53%). These findings demonstrated that **Cu-MOF-COOH** nanosheets achieve optimal dispersion in toluene and exhibit the desired extraction effect. Consequently, toluene was chosen as the organic phase for further investigation.

pH effect study

The MOF nanosheets (7 mg) was dispersed in 10 mL toluene and added to 15 mL of 10 ppm Sr^{2+} solution. The extraction test was conducted under different pH conditions (ranging from 3.0 to 10.0) adjusted by HNO_3 or NaOH solutions. The mixture was then stirred for 12 hours. After extraction, the mixture was allowed to stand for 12 hours to separate the two phases. The samples were filtered through a 0.22 μm membrane filter. Finally, the Sr^{2+} concentration was determined by AAS or ICP-MS.

Kinetics study

At room temperature, 7 mg of MOF nanosheets was dispersed in 10 mL toluene and added to 15 mL of 5 ppm Sr^{2+} solution at pH 10.0. The mixture was then stirred for a certain time. After extraction, the samples were filtered through a 0.22 μm membrane filter. Finally, the Sr^{2+} concentration was determined by AAS or ICP-MS. The kinetics of 3D bulk **Cu-MOF-COOH** in Sr^{2+} solution was tested by a similar method.

Isothermal performance study

In a typical experiment, 5 mg of MOF nanosheets was dispersed in 10 mL toluene solution and added to 60 mL Sr^{2+} solution with the concentration of X ppm (X = 5, 10, 20, 30, 40, 60, 70, 80 ppm), then the mixture was stirred 12 hours at room temperature. The extraction experiments were conducted at pH 10.0. After extraction, the mixture was allowed to stand for 12 hours to separate the two phases. The samples were filtered through a 0.22 μm membrane filter. Finally, the Sr^{2+} concentration was determined by AAS or ICP-MS. A similar method was used to study the extraction behavior of 3D bulk **Cu-MOF-COOH** in solutions with different initial Sr^{2+} concentrations.

Selective extraction experiment

The MOF nanosheets (7 mg) was dispersed in 10 mL toluene and added to 15 mL aqueous solutions with different metal ions (10 ppm) of Sr^{2+}, Na^+, K^+, Rb^+, Cs^+, Ca^{2+}, Mg^{2+} and Ba^{2+}, respectively. The extraction experiments were conducted at pH 10.0. The mixture was then stirred for 8 hours. After extraction, the mixture was allowed to stand for 12 hours to separate the two phases. The samples were filtered through 0.22 μm membrane filters, and finally the Sr^{2+} concentration was determined by AAS and ICP-MS. The extraction selectivity of 3D bulk **Cu-MOF-COOH** and H_4L ligand was investigated in a similar way.

Competing extraction study

The 5 ppm Sr^{2+} solution was mixed with single interfering ions at concentrations of 5 ppm, 50 ppm, and 250 ppm, including Na^+, K^+, Rb^+, Cs^+, Mg^{2+}, Ca^{2+}, and Ba^{2+}. Subsequently, 7 mg of MOF nanosheets were dispersed in 10 mL of toluene and added to 15 mL of mixed solution containing different concentrations and types of interfering ions at pH 8.0. The mixture was stirred at room temperature for 12 hours. After extraction, the mixture was allowed to stand for 12 hours to separate the two phases. The samples were then filtered through 0.22 μm membrane filters, and the Sr^{2+} concentration was determined by AAS and ICP-MS. The 5 ppm Sr^{2+} solution was mixed with a solution containing 1-20 times all the aforementioned metal ions. Subsequently, 30 mg of MOF nanosheets were dispersed in 10 mL of toluene and added to 15 mL of mixed solution containing different concentrations of interfering ions at pH 8.0. The subsequent steps were carried out as described above.

Extraction experiment in actual water samples

30 mg of MOF nanosheets was dispersed in 10 mL toluene and added to 15 mL each of tap water, lake water, simulated groundwater, and simulated low-level radioactive wastewater, which had been spiked with 5 ppm of Sr^{2+}, respectively. The tap water is supplied by the Yantai Qingquan Industrial Co. and the lake water is sourced from the Sanyuan Lake at Yantai University. The simulated groundwater and simulated low-level radioactive wastewater were prepared according to the literature.[2, 3] The above-mentioned water samples were filtered through a 0.22 μm filter membrane before conducting the extraction experiment. The solution was stirred for 12 hours at room temperature. After the extraction reached equilibrium, the mixture was allowed to stand for 12 hours to separate the two phases. The samples were then filtered through a 0.22 μm membrane filter, and the Sr^{2+} concentration was determined by AAS and ICP-MS.

Regeneration experiment

The recyclability was evaluated through the regeneration test. In each cycle, the Sr^{2+}-loaded MOF nanosheets were separated by the centrifugation and immersed in a glass beaker containing 15mL of 0.01 M Na_2HPO_4 solution for elution. After immersion in the 0.01 M Na_2HPO_4 solution for 12 hours, the samples were washed three times with deionized water and dried in preparation for the subsequent test.

The kinetics data were fitted with a pseudo first-order model, and pseudo-second-order, which are expressed as follows:

$$ln(q_e - q_t) = lnq_e - k_1 t \qquad (S1)$$

$$\frac{t}{q_t} = \frac{1}{k_2 q_e^2} + \frac{t}{q_e} \qquad (S2)$$

where q_t (mg g^{-1}) and q_e (mg g^{-1}) are the extraction capacity at any time t (minutes) and at equilibrium; k_1 (s^{-1}) and k_2 (g mg^{-1} s^{-1}) are kinetic rate constants for the pseudo-first-order and pseudo-second-order models, respectively.

The Langmuir and Freundlich isotherm models were employed to simulate the isotherm data and can be described as:

$$\frac{C_e}{q_e} = \frac{C_e}{q_m} + \frac{1}{q_m K_L} \qquad (S3)$$

$$lnq_e = lnK_F + \frac{1}{n} C_e \qquad (S4)$$

where q_e (mg g^{-1}) is the extraction amounts at equilibrium and C_e (mg L^{-1}) is the equilibrium concentration. q_m (mg g^{-1}) is the maximum amount or the saturated extraction amount. K_L (L mg^{-1}) is the Langmuir constant, quantitatively reflecting the affinity of binding sites to energy of extraction. K_F ((mg g^{-1})/(L mg^{-1})$^{1/n}$) is the Freundlich constant which indicates the extraction capacity and n is an empirical parameter related to the intensity of extraction. The Langmuir model assumes that the active site on the solid surface can only be occupied by one layer, and there is no interaction between extract molecules. In contrast, the Freundlich model is heterogeneous.

Calculation method

The Forcite model calculation was performed to better elucidate the electronic and structural properties and atomic interactions between Sr^{2+} and MOF nanosheets. The cage-like cavity unit is suitable as model for **Cu-MOF-COOH** due to the time-consuming nature of model calculations. The binding behavior between MOF nanosheets and Sr^{2+} was determined and optimized by Model in Materials Studio 2023 using the condensed-phase optimized molecular potentials for atomistic simulation studies (COMPASS III) force field. The convergence quality was set as fine, in which the energy was 1×10^{-4} kcal/mol, the maximum force was 0.005 kcal/mol/Å, the maximum iteration was set to 10000. The binding energies of cage-like cavity with Sr^{2+} were calculated by the following equation:

$$\Delta E_b = E_{(cage+M^{n+})} - E_{(cage)} - E[_{(M(H2O)m^{n+})}]$$

where $E_{(cage+M^{n+})}$, $E_{(cage)}$, and $E[_{(M(H2O)m^{n+})}]$ represent the total energy of metal ions on cage, cage, and hydrated metal ions, respectively. $M^{n+} = Sr^{2+}$, Na^+, K^+, Rb^+, Cs^+, Mg^{2+}, Ca^{2+}, and Ba^{2+}.

Supporting Tables

Table S1. The Cu^{2+} leaching rate of 2D **Cu-MOF-COOH** nanosheets under different conditions.

	pH	Cu^{2+} leaching rate
Aqueous phase	1.0	2.16%
	2.0	1.31%
	3.0	0.27%
	5.0	0.13%
	7.0	0.01%
	9.0	0.09%
	10.0	0.06%
	12.0	0.73%
	13.0	3.31%
Toluene	-	0.00%
Aqueous phase after extraction	10.0	0.13%
Toluene phase after extraction	-	0.24%

Table S2. Kinetic parameters of extraction of Sr^{2+} by 2D **Cu-MOF-COOH** nanosheets and 3D **Cu-MOF-COOH**.

			Pseudo-first-order model			Pseudo-second-order model		
	T/K	$q_{e,exp}$	k_1	$q_{e,cal}$	R^2	k_2	$q_{e,cal}$	R^2
2D Cu-MOF-COOH	298	0.164	0.143	2.461	0.796	0.390	10.232	0.999
3D Cu-MOF-COOH	298	8.927	0.144	1.796	0.509	0.199	16.60	0.998

Table S3. Comparison of Sr^{2+} maximum uptake capacities for 2D **Cu-MOF-COOH** nanosheets and 3D **Cu-MOF-COOH** with other materials.

Materials	Maximum uptake capacity (mg/g)	References
ZrP	102.9	4
CA@ZrP (90%)	72.99	4
FZU-1	62.8	5
1D-K_2SbPO_6	175.90	6
K-NGH-1	41.62	7
M-Sn-Se	104.17	8
SbS-1K	61.16	9
SZ-4	117.9	10
LTO-MX PAN	24.05	11
Ca-ZrP	226.9	12
InS-1	105.3	13
SZ-4	121	14
DGIST-12	41.1	15
FJSM-SnS-2	59.4	16
FJSM-SnS-3	57.8	16
FJSM-GAS-1	80	17
MOF-18Cr6	84.93	18
3D Cu-MOF-COOH	**147.79**	**this work**
2D Cu-MOF-COOH nanosheets	**231.72**	**this work**

Table S4. Isotherm parameters of 2D **Cu-MOF-COOH** nanosheets and 3D **Cu-MOF-COO**H for extraction of Sr^{2+}.

	Langmuir			Freundlich		
	q_{max}	K_L	R^2	K_F	n	R^2
2D Cu-MOF-COOH	257.069	0.166	0.999	69.722	3.147	0.942
3D Cu-MOF-COOH	161.550	0.197	0.992	39.075	2.815	0.851

Supporting Scheme and Figures

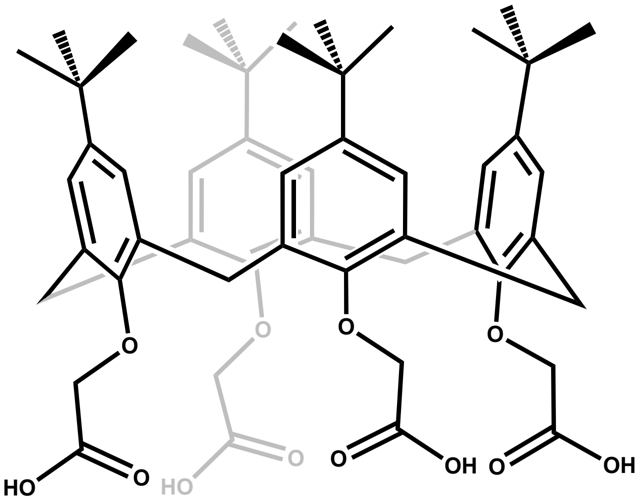

Scheme S1. The molecular structure of H_4L ligand.

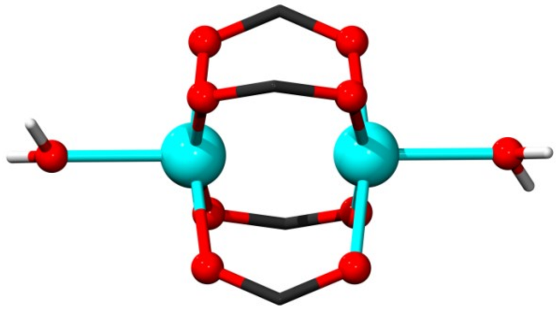

Figure S1. The paddle-wheel unit $[Cu_2(COO)_4(H_2O)_2]$ in **Cu-MOF-COOH**.

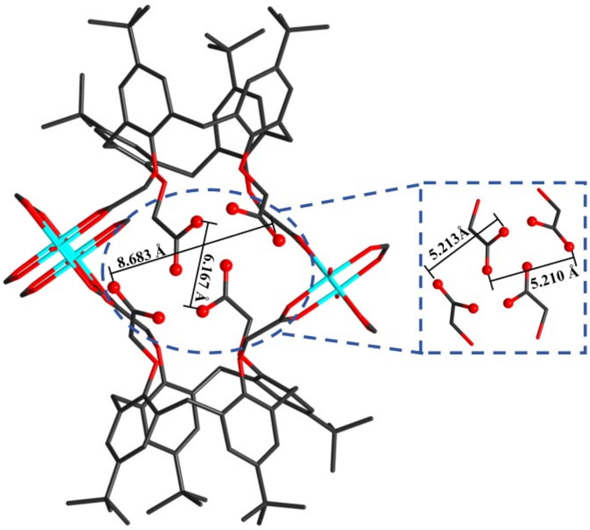

Figure S2. The potential binding sites of the uncoordinated carboxylate groups in **Cu-MOF-COOH** nanosheet.

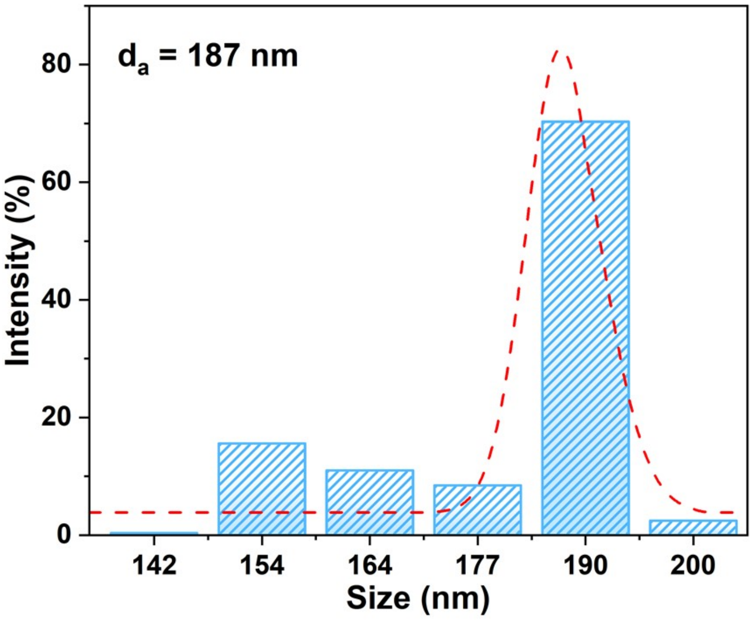

Figure S3. The particle size distribution of **Cu-MOF-COOH** nanosheets, measured by dynamic light scattering (DLS) in MeOH/isopropanol (4/1, V/V) at 25 °C.

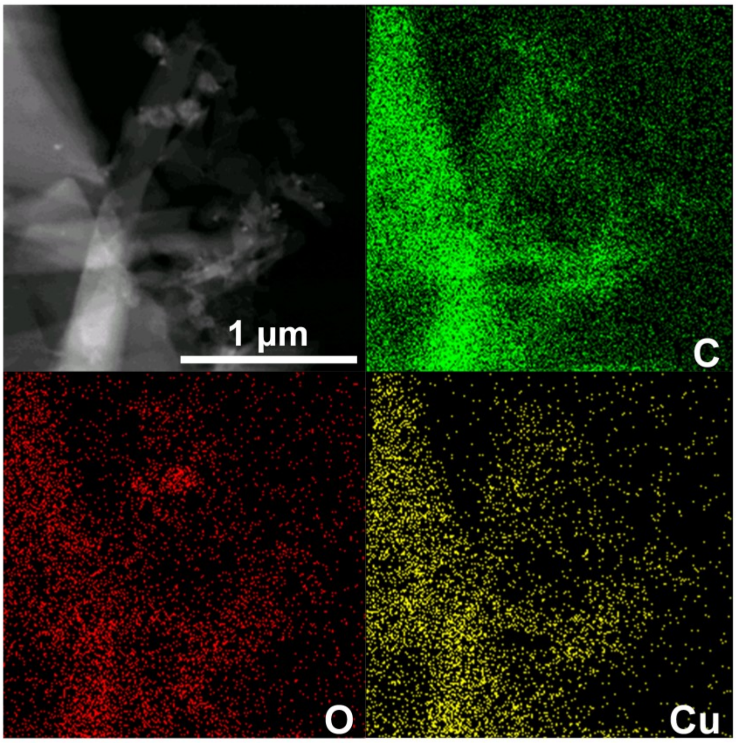

Figure S4. Elemental mapping images of **Cu-MOF-COOH** nanosheets.

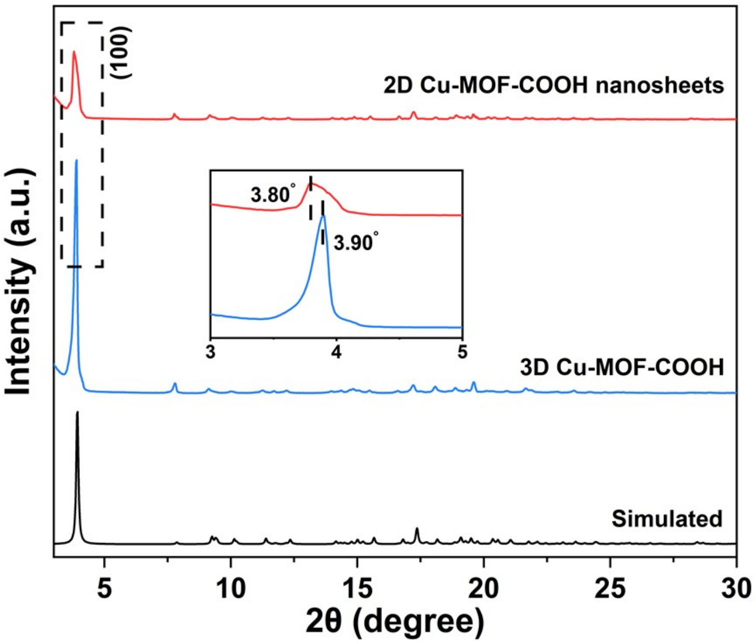

Figure S5. The PXRD patterns of the simulated **Cu-MOF-COOH**, as-synthesized 3D **Cu-MOF-COOH** and **Cu-MOF-COOH** nanosheets.

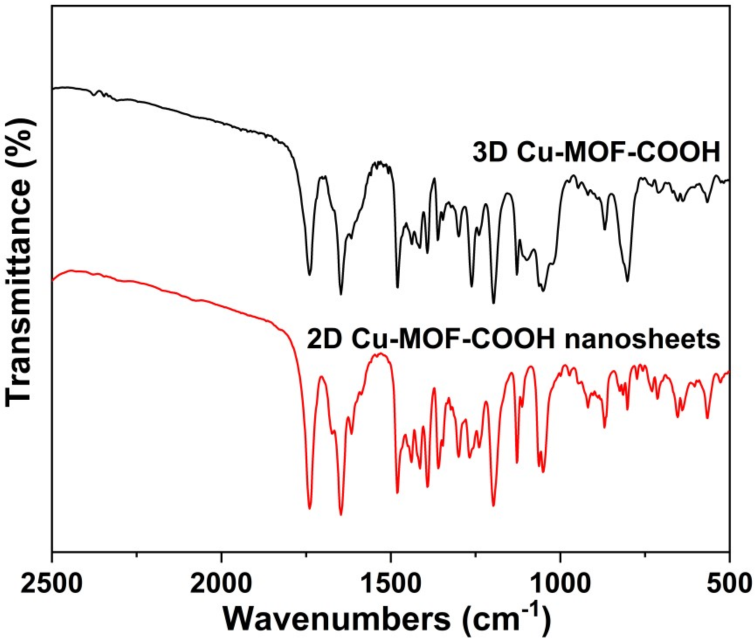

Figure S6. FT-IR spectra of 3D **Cu-MOF-COOH** and **Cu-MOF-COOH** nanosheets.

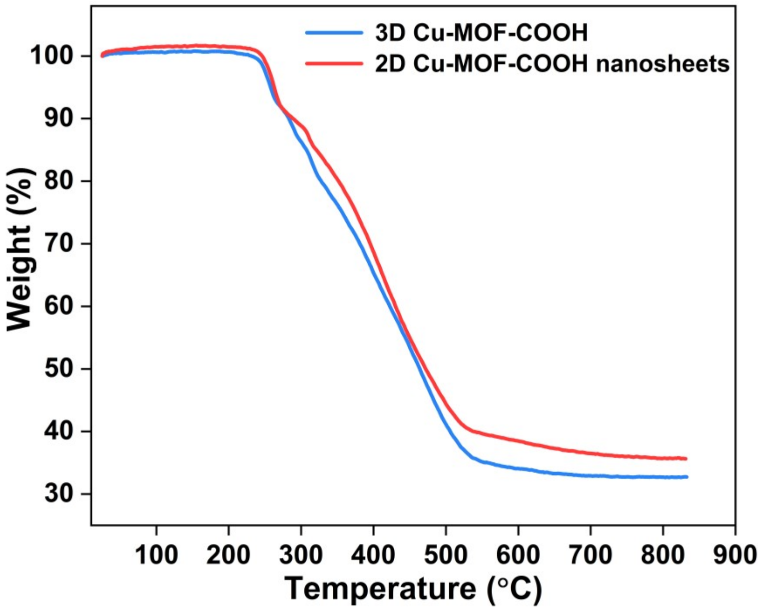

Figure S7. TGA curves of 3D **Cu-MOF-COOH** and **Cu-MOF-COOH** nanosheets.

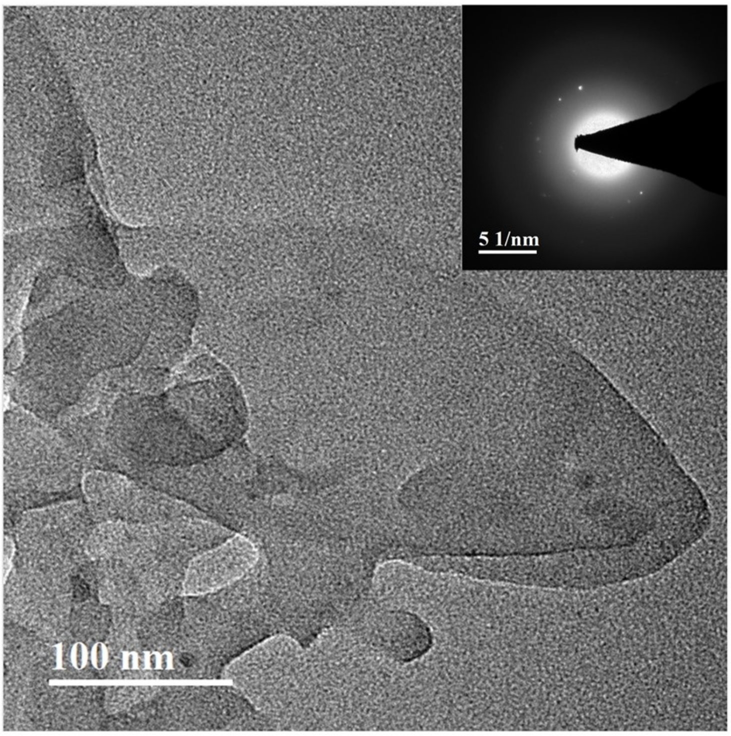

Figure S8. (a) TEM image and SAED patterns of **Cu-MOF-COOH** nanosheets.

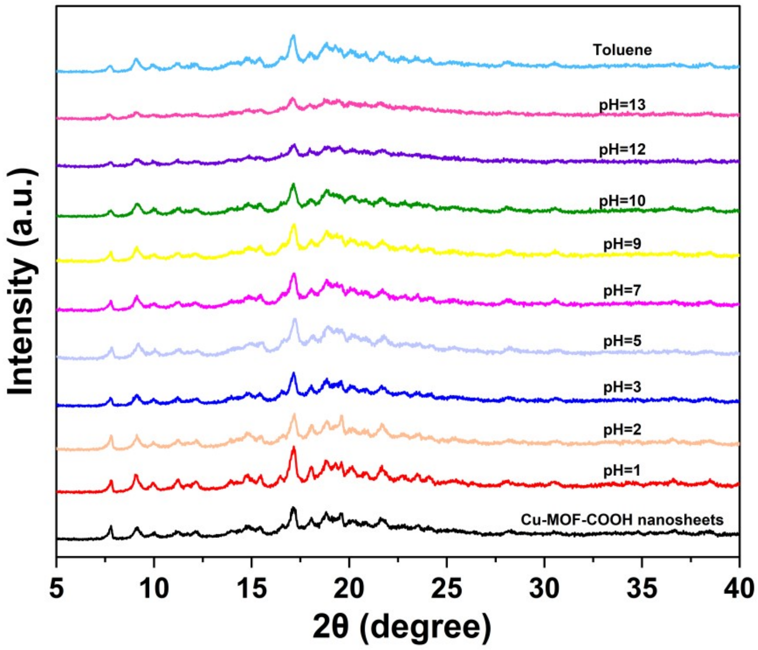

Figure S9. PXRD patterns of **Cu-MOF-COOH** nanosheets after soaking in aqueous solution at pH = 1, 2, 3, 5, 7, 9, 10, 12, 13 and toluene for 12 hours.

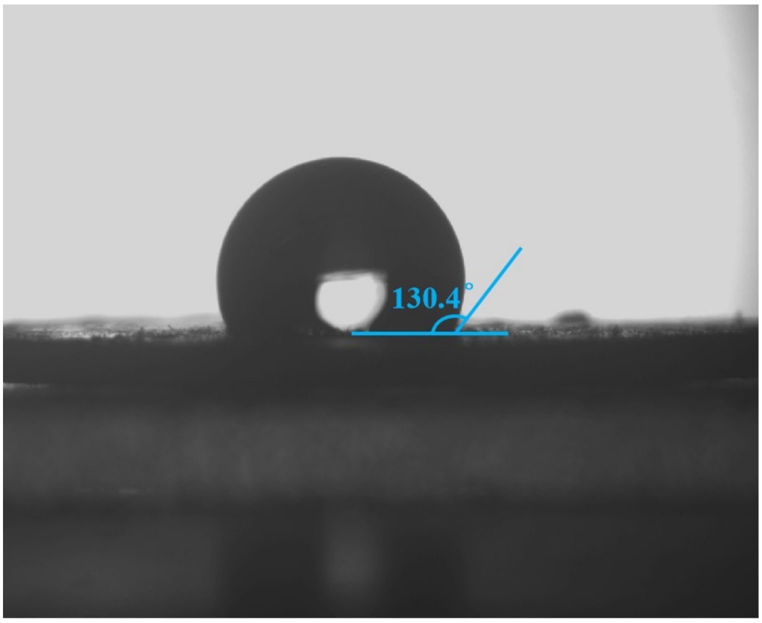

Figure S10. Contact angle of **Cu-MOF-COOH** nanosheets.

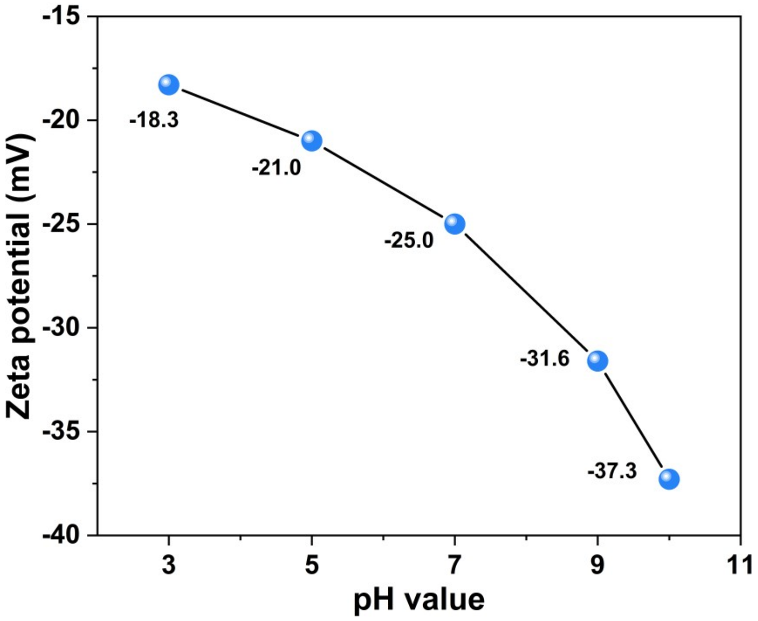

Figure S11. Zeta potentials of **Cu-MOF-COOH** nanosheets in aqueous solution with different pH values.

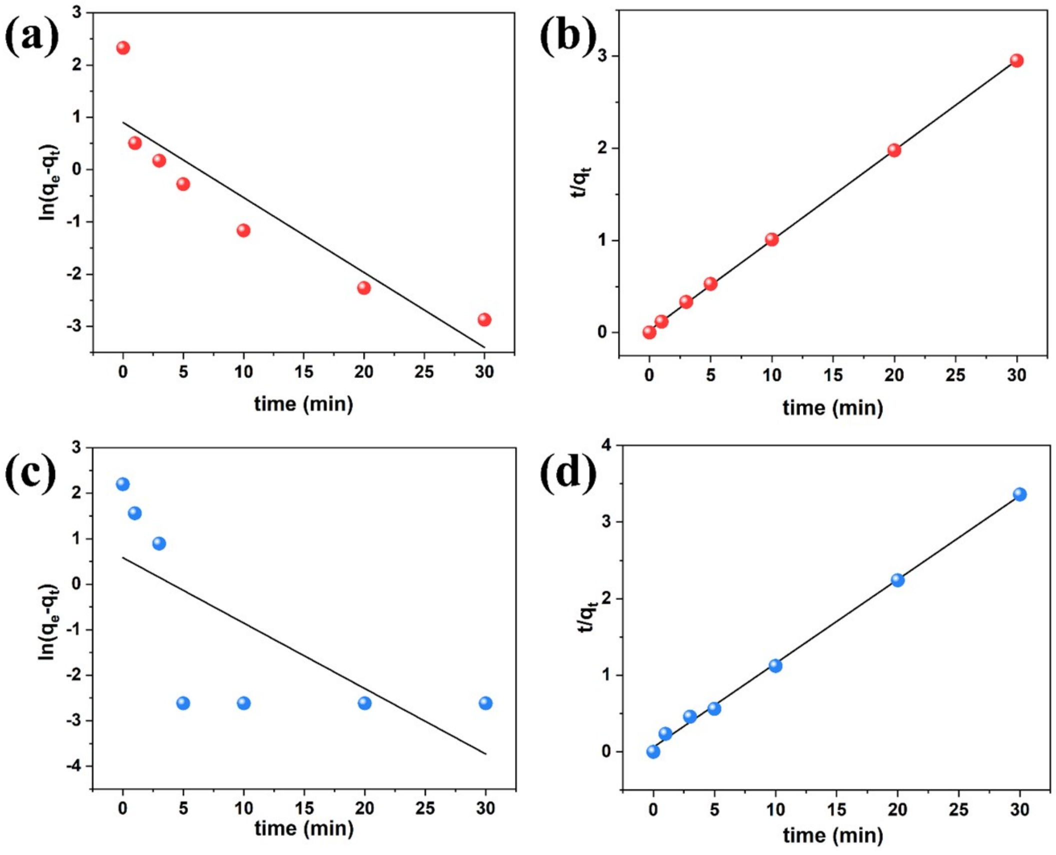

Figure S12. Pseudo-first-order (a) and pseudo-second-order (b) kinetic modes fitting for Sr^{2+} extraction by **Cu-MOF-COOH** nanosheets. Pseudo-first-order (c) and pseudo-second-order (d) kinetic modes fitting for Sr^{2+} extraction by 3D **Cu-MOF-COOH**.

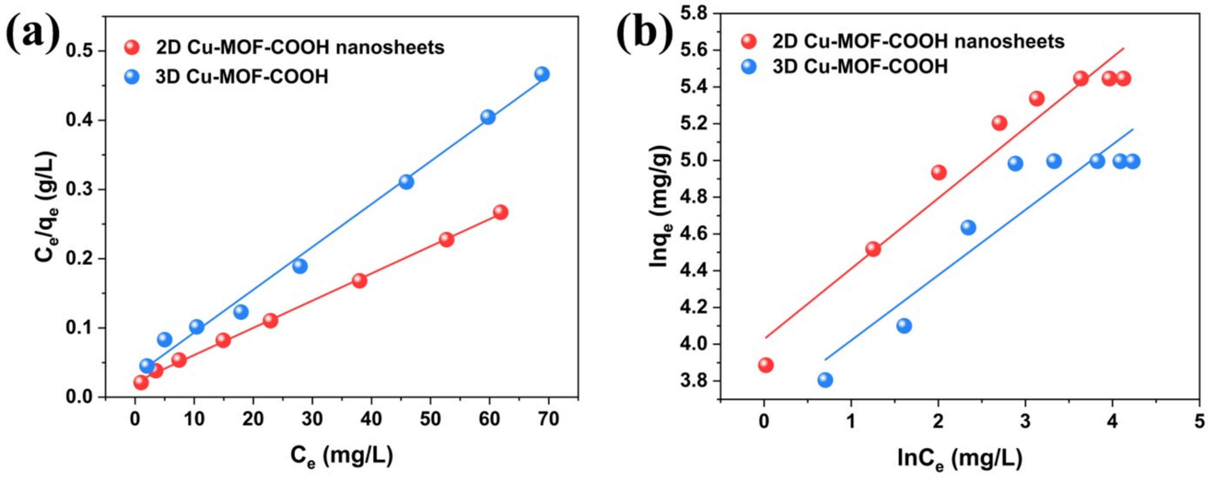

Figure S13. Langmuir (a) and Freundlich (b) isotherm models fitting for Sr^{2+} capture by **Cu-MOF-COOH** nanosheets and 3D **Cu-MOF-COOH**.

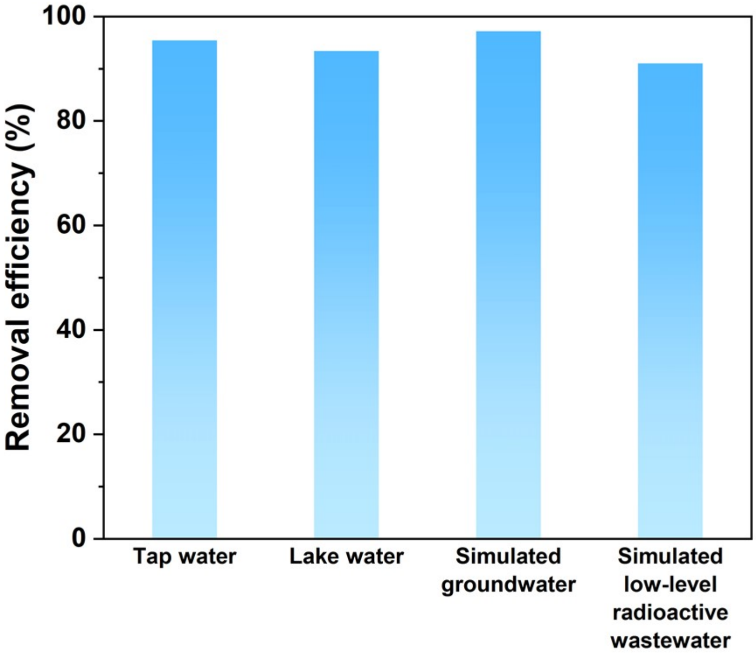

Figure S14. Removal efficiency of **Cu-MOF-COOH** nanosheets for Sr^{2+} in the various actual water samples.

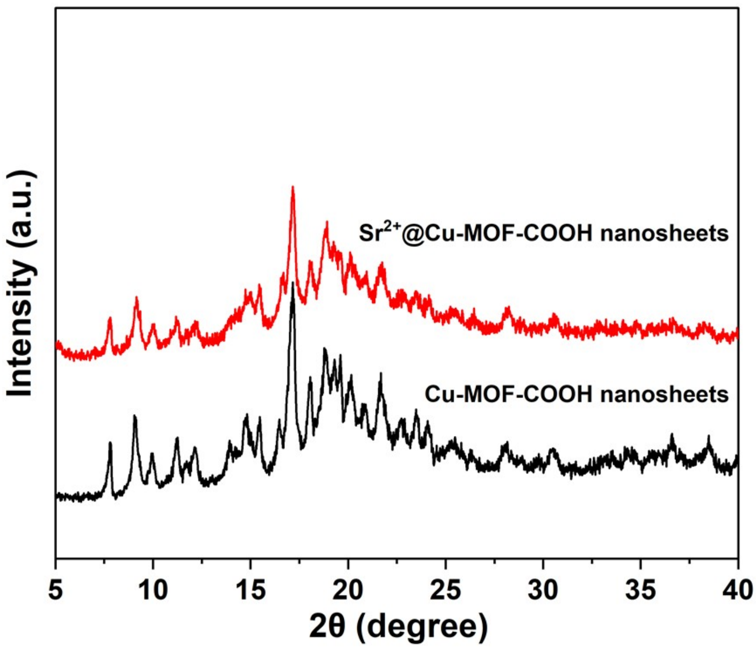

Figure S15. PXRD patterns of **Cu-MOF-COOH** nanosheets before and after Sr^{2+} extraction.

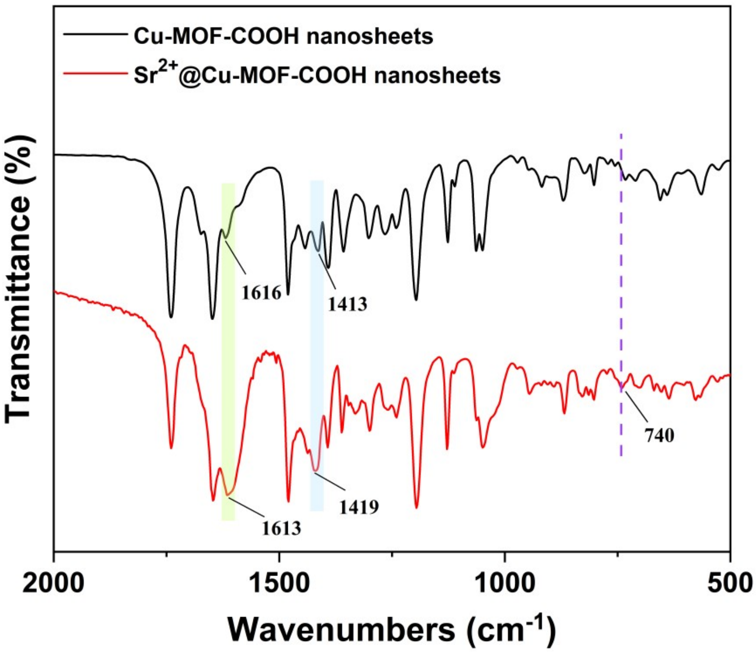

Figure S16. Comparison of the FT-IR spectra for **Cu-MOF-COOH** nanosheets after soaking pH =10.0 solution and Sr^{2+}@**Cu-MOF-COOH** nanosheets.

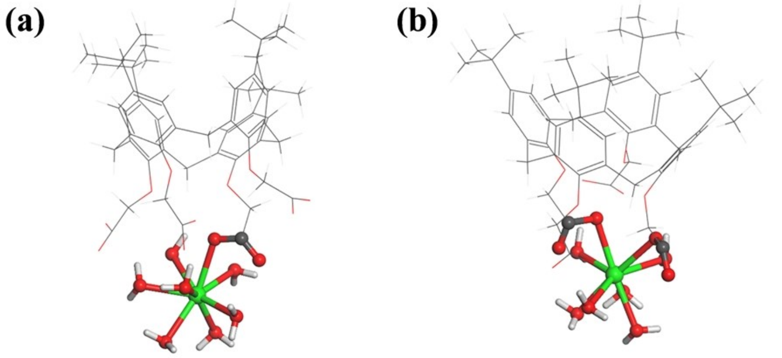

Model 1
E_b= -0.56 eV
Sr-O (COO^-): 2.613 Å

Model 2
E_b= -1.07 eV
Sr-O (COO^-): 2.592~2.628 Å

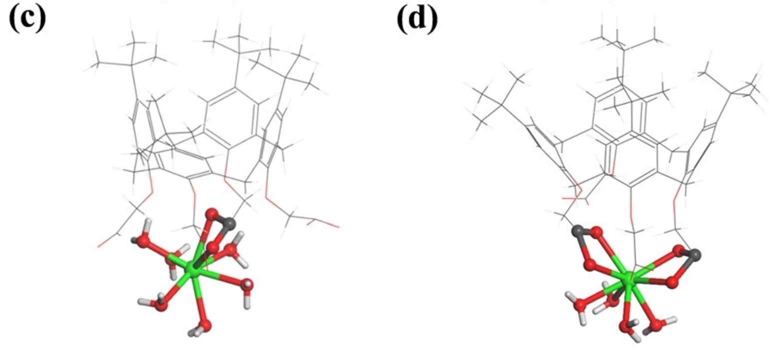

Model 3-a
E_b= -1.18 eV
Sr-O (COO^-): 2.582~2.613 Å

Model 3-b
E_b= -1.95 eV
Sr-O (COO^-): 2.625~2.637 Å

Figure S17. Model calculation for Sr^{2+} capture by H_4L ligand.

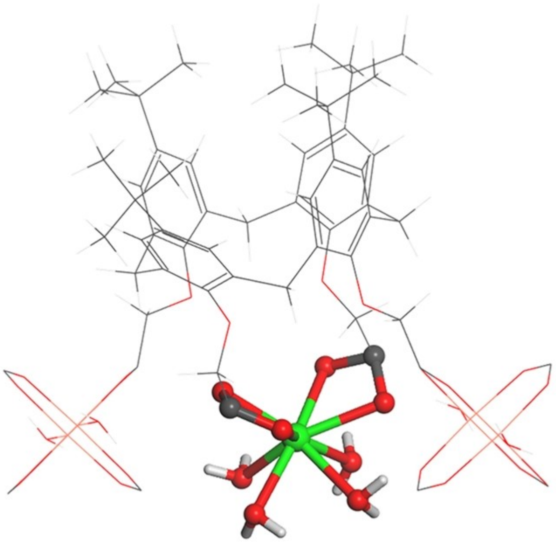

E_b= -1.34 eV
Sr-O (COO^-): 2.569~2.609 Å

Figure S18. Sr^{2+} binding model without cage-like cavity.

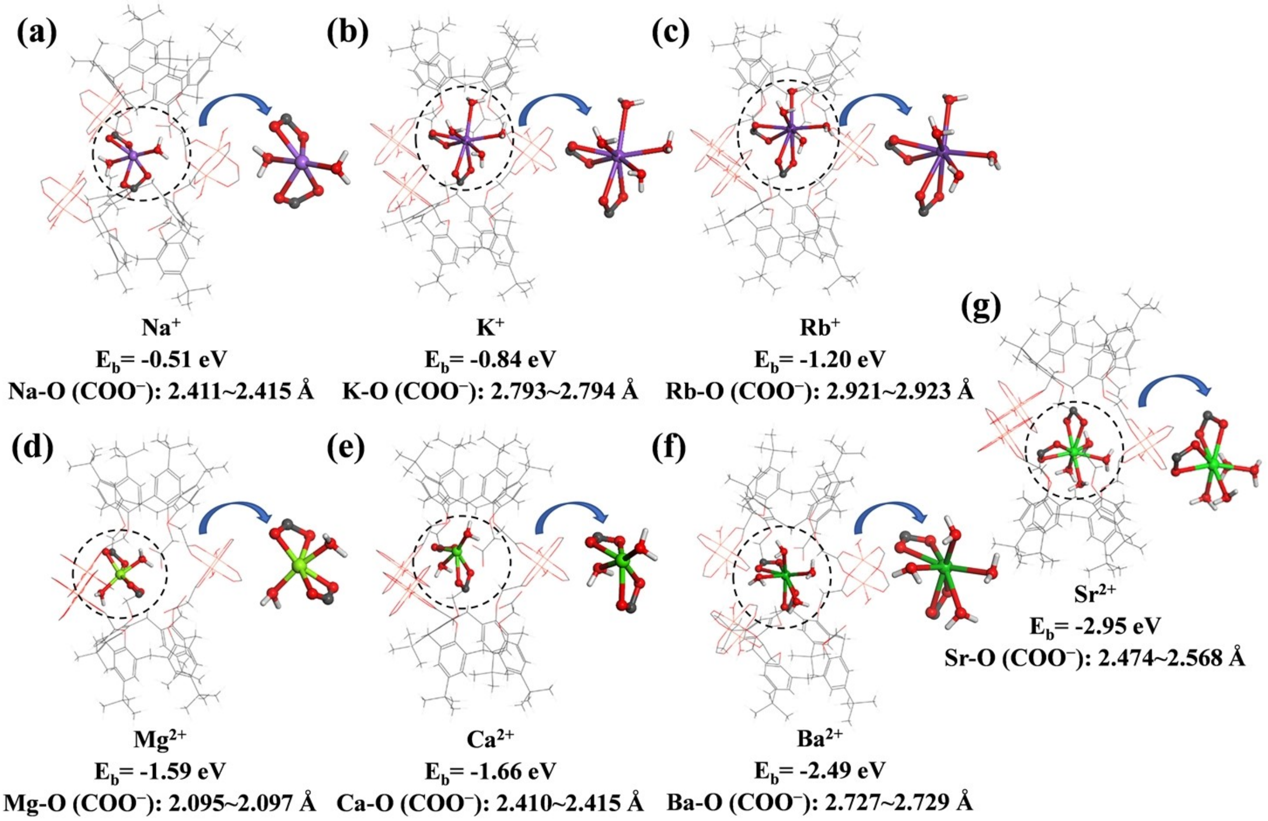

Na^+
E_b= -0.51 eV
Na-O (COO^-): 2.411~2.415 Å

K^+
E_b= -0.84 eV
K-O (COO^-): 2.793~2.794 Å

Rb^+
E_b= -1.20 eV
Rb-O (COO^-): 2.921~2.923 Å

Sr^{2+}
E_b= -2.95 eV
Sr-O (COO^-): 2.474~2.568 Å

Mg^{2+}
E_b= -1.59 eV
Mg-O (COO^-): 2.095~2.097 Å

Ca^{2+}
E_b= -1.66 eV
Ca-O (COO^-): 2.410~2.415 Å

Ba^{2+}
E_b= -2.49 eV
Ba-O (COO^-): 2.727~2.729 Å

Figure S19. Theoretical model calculation for metal ions of Na^+, K^+, Rb^+, Mg^{2+}, Ca^{2+}, Ba^{2+} and Sr^{2+}.

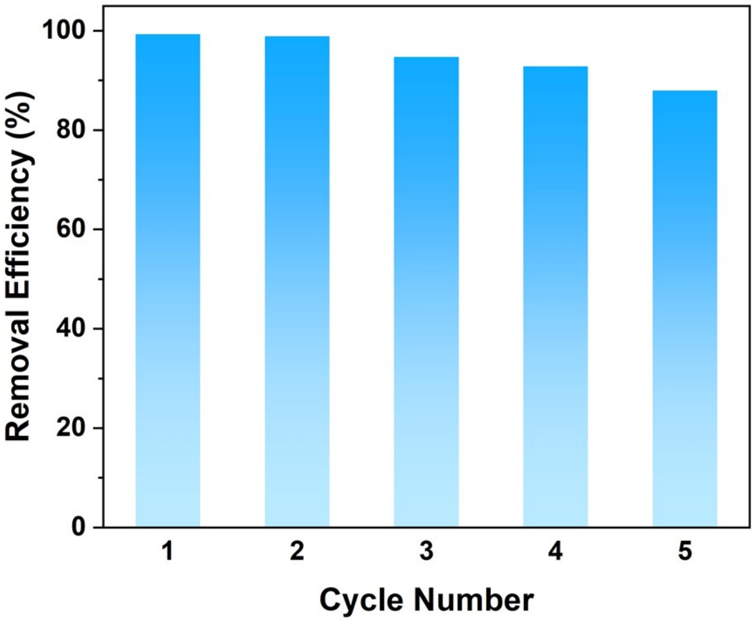

Figure S20. Reusability of **Cu-MOF-COOH** nanosheets for Sr^{2+} extraction.

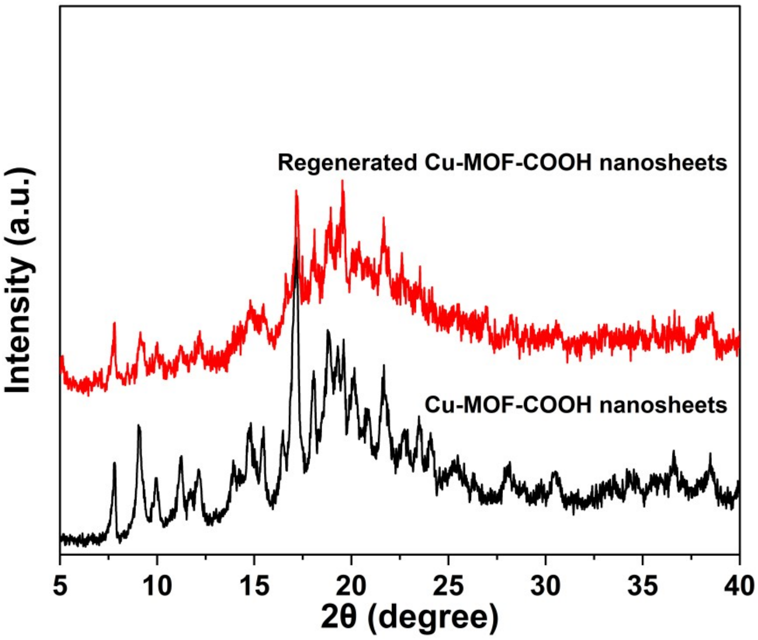

Figure S21. PXRD patterns of **Cu-MOF-COOH** nanosheets and regenerated **Cu-MOF-COOH** nanosheets.

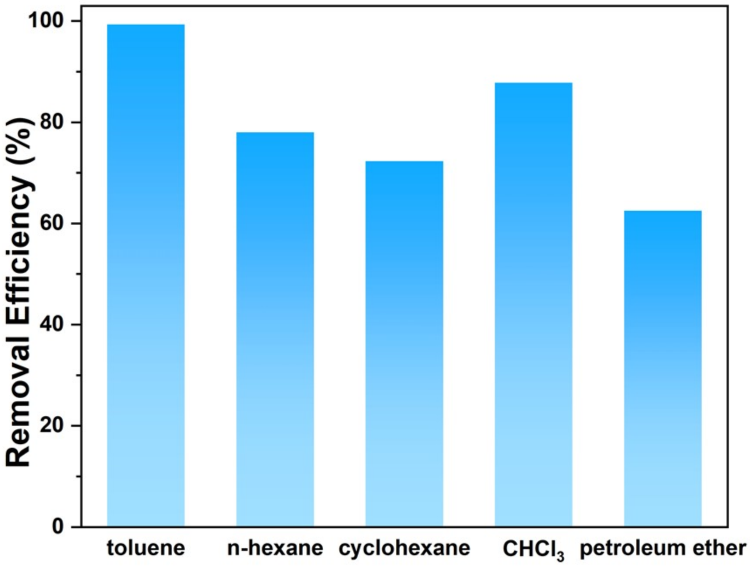

Figure S22. Influence of various organic phases on the extraction of Sr^{2+} by the **Cu-MOF-COOH** nanosheets.

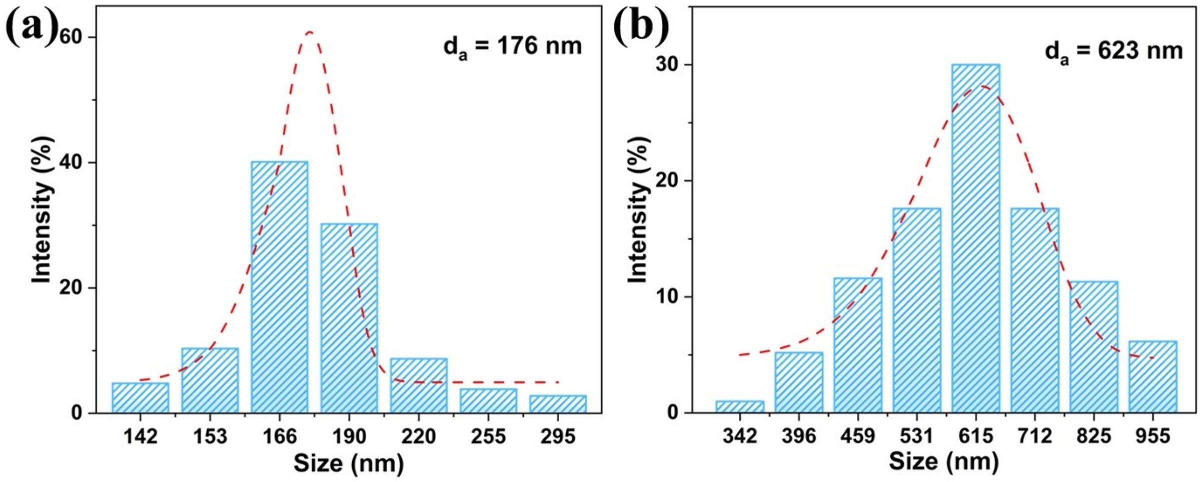

Figure S23. The particle size distribution of **Cu-MOF-COOH** nanosheets, measured by DLS in (a) toluene and (b) aqueous solution at 25 °C.

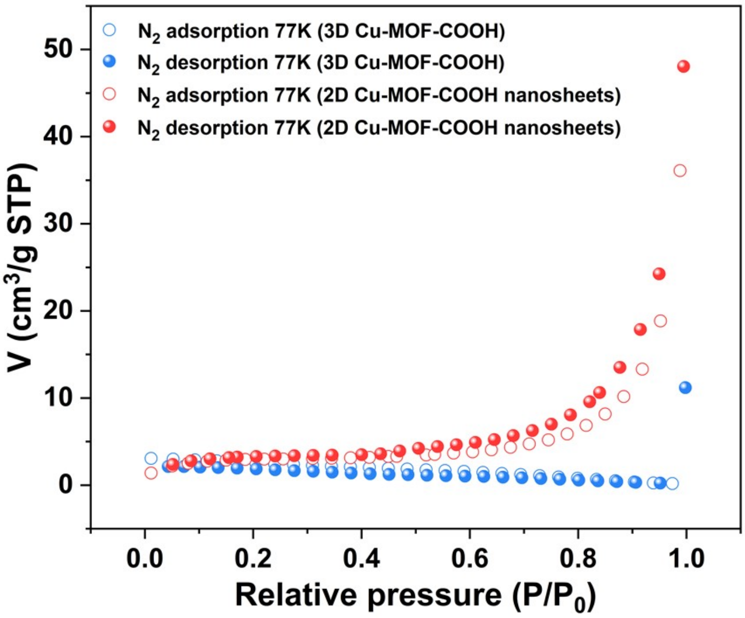

Figure S24. N_2 adsorption and desorption isotherms for 3D **Cu-MOF-COOH** and **Cu-MOF-COOH** nanosheets.

References

(1) Sun, H.; Wang, K.-Z.; Yao, M.-R.; Yu, C.-X.; Song, Y.-H.; Ding, J.; Zhou, Y.-L.; Liu, D.; Liu, L.-L. Fabrication of ultrathin two-dimensional MOF nanosheets with cage-like cavities showing excellent adsorption for lead(II). *Inorg. Chem. Front.* **2023**, *10*, 6566-6577.

(2) Datta, S. J.; Moon, W. K.; Choi, D. Y.; Hwang, I. C.; Yoon, K. B. A novel vanadosilicate with hexadeca-coordinated Cs^+ ions as a highly effective Cs^+ remover. *Angew. Chem. Int. Ed.* **2014**, *53*, 7203-7208.

(3) Yin, J.; Yang, S.; He, W.; Zhao, T.; Li, C.; Hua, D. Biogene-derived aerogels for simultaneously selective adsorption of uranium(VI) and strontium(II) by co-imprinting method. *Sep. Purif. Technol.* **2021**, *271*, 118849.

(4) Liu, R.; Chen, G.; Wang, Z.; Zhao, Q.; Wu, L.; Li, Q.; Tian, R.; Chen, X.; Li, X.; Chen, Z.; Zhu, L.; Chen, J.; Duan, T. Calcium-intercalated zirconium phosphate by granulation: A strategy for enhancing adsorption selectivity of strontium and cesium from liquid radioactive waste. *Inorg. Chem.* **2023**, *62*, 5799-5809.

(5) Liu, Y.-X.; Wu, P.-X.; Dai, J.-Y.; Cai, P.-W.; Sun, C.; Zheng, S.-T. Site differentiation strategy for selective strontium uptake and elution within an all-inorganic polyoxoniobate framework. *Nat. Commun.* **2024**, *15*, 8896.

(6) Guo, Y.-L.; Sun, H.-Y.; Zeng, X.; Lv, T.-T.; Yao, Y.-X.; Zhuang, T.-H.; Feng, M.-L.; Huang, X.-Y. Efficient removal of Sr^{2+} ions by a one-dimensional potassium phosphatoantimonate. *Chem. Eng. J.* **2023**, *460*, 141697.

(7) Sun, H.-Y.; Hu, B.; Lv, T.-T.; Guo, Y.-L.; Yao, Y.-X.; Yang, L.; Feng, M.-L.; Huang, X.-Y. Efficient Co-adsorption and highly selective separation of Cs^+ and Sr^{2+} with a K^+-activated niobium germanate by the pH control. *Small* **2023**, *19*, 2208212.

(8) Wang, K.-Y.; Liu, Y.; Zhu, J.-Y.; Cheng, L.; Wang, C. M-Sn-Q (M = Zn, Cd; Q = S, Se) compounds templated by (Alkyl)ammonium species: Synthesis, crystal structure, and Sr^{2+} adsorption property. *Inorg. Chem.* **2022**, *61*, 19106-19118.

(9) Zhao, Y.-M.; Cheng, L.; Wang, K.-Y.; Hao, X.; Wang, J.; Zhu, J.-Y.; Sun, M.; Wang, C. pH-controlled switch over coadsorption and separation for mixed Cs^+ and Sr^{2+} by an acid-resistant potassium thioantimonate. *Adv. Funct. Mater.* **2022**, *32*, 2112717.

(10) Zhang, J.; Chen, L.; Dai, X.; Zhu, L.; Xiao, C.; Xu, L.; Zhang, Z.; Alekseev, E. V.; Wang, Y.; Zhang, C.; Zhang, H.; Wang, Y.; Diwu, J.; Chai, Z.; Wang, S. Distinctive two-step intercalation of Sr^{2+} into a coordination polymer with record high ^{90}Sr uptake capabilities. *Chem* **2019**, *5*, 977-994.

(11) Lim, Y.; Lee, D. S. Effective radioactive strontium removal using lithium titanate decorated $Ti_3C_2T_x$ MXene/polyacrylonitrile beads. *J. Hazard. Mater.* **2024**, *475*, 134919.

(12) Liu, R.; Zhao, Q.; Wang, Z.; Jiang, R.; Lin, C.; Wu, L.; Chen, G.; He, P.; Zhu, L.; Chen, J.; Duan, T. Regulating the interlayer spacing of $Ca_{0.55}ZrH_{0.9}(PO_4)_2$ for selective removal of Sr^{2+} from acidic wastewater. *J. Mater. Chem. A* **2024**, *12*, 14608-14618.

(13) Wang, K.-Y.; Sun, M.; Ding, D.; Liu, H.-W.; Cheng, L.; Wang, C. Di-lacunary $[In_6S_{15}]^{12-}$ cluster: the building block of a highly negatively charged framework for superior Sr^{2+} adsorption capacities. *Chem. Commun.* **2020**, *56*, 3409-3412.

(14) Garai, M.; Yavuz, C. T. Radioactive strontium removal from seawater by a MOF via two-step ion exchange. *Chem* **2019**, *5*, 750-752.

(15) Kim, Y.; Jin, K.; Park, I.-H.; Lee, S.; Park, J.; Park, J. Selective Sr^{2+} capture in an In^{3+}-based anionic metal-organic framework. *Chem. Eng. J.* **2024**, *484*, 149321.

(16) Li, W.-A.; Li, J.-R.; Zhang, B.; Sun, H.-Y.; Jin, J.-C.; Huang, X.-Y.; Feng, M.-L. Layered thiostannates with distinct arrangements of mixed cations for the selective capture of Cs^+, Sr^{2+}, and Eu^{3+} ions. *ACS Appl. Mater. Interfaces* **2021**, *13*, 10191-10201.

(17) Feng, M.-L.; Sarma, D.; Gao, Y.-J.; Qi, X.-H.; Li, W.-A.; Huang, X.-Y.; Kanatzidis, M. G. Efficient removal of UO_2^{2+}, Cs^+, and Sr^{2+} ions by radiation-resistant gallium thioantimonates. *J. Am. Chem. Soc.* **2018**, *140*, 11133-11140.

(18) Feng, L.; Chen, X.; Cao, M.; Zhao, S.; Wang, H.; Chen, D.; Ma, Y.; Liu, T.; Wang, N.; Yuan, Y. Decorating channel walls in metal-organic frameworks with crown ethers for efficient and selective separation of radioactive strontium(II). *Angew. Chem. Int. Ed.* **2023**, *62*, e202312894.